# Nonlinear absorption and phase shift in coupled optical cavities

T. Hasegawa*

*Department of Physics, Keio University, Kanagawa 223-8522, Japan*

(Received 15 March 2015; published 13 October 2015)

The nonlinear absorption process and associated phase shift in coupled optical cavities are studied experimentally by observing optical resonance properties. In the coupled cavity configuration, two optical cavities, one for a fundamental beam and the other for a second-harmonic (SH) beam, are coupled by a nonlinear crystal for the second-harmonic generation (SHG). The cavity for the SH beam effectively extends the nonlinear crystal length so that the frequency-conversion efficiency of the SHG, which is proportional to the square of the crystal length, is enhanced. In the observation, power reduction of the fundamental beam at resonance is observed as a small dip in the resonance curve. According to a model calculation, it is found that this power reduction is caused by blue-induced infrared absorption.

DOI: 10.1103/PhysRevA.92.043815 PACS number(s): 42.65.Ky, 42.60.Da, 79.20.Ws

## I. INTRODUCTION

Enhancement of second-harmonic generation (SHG) in optical cavities in which both the fundamental beam and the second harmonic (SH) beam are resonant simultaneously has been studied. The SH beam is coupled with the fundamental beam through the nonlinear crystal (NLC) for the SHG, and the cavity for the SH beam effectively extends the nonlinear crystal length. Hence the SHG efficiency can be enhanced substantially.

Doubly resonant monolithic optical cavities in which both the fundamental beam and the SH beam can be simultaneously resonant in a single cavity have advantages in mechanical stability. The SHG enhancement in the macroscopic doubly resonant cavities has been demonstrated and studied [1–3], and later microscopic monolithic doubly resonant cavities are extensively studied experimentally [4–8] and theoretically [9–13] because of high nonlinearity in addition to the mechanical stability. Examples are planar microcavities [7,10,12], microdisk cavities [4,9,11], and photonic crystal cavities [5,6]. It is also suggested that the third-harmonic generation can be enhanced [13]. In the case of coupled optical cavities [14] in which the fundamental and the SH beams are in two spatially separated optical cavities with a shared optical path with the NLC, cavity design is less restricted compared to the double-resonant configuration because dispersion compensation is unnecessary. In addition, any kind of NLC can be used, and hence application to any range of wavelength is possible. As an important application, this setup can be easily applied to the fourth-harmonic generation by inserting another NLC in the cavity for the SH beam [15,16]. As a drawback, the size of the cavities tends to be large compared to the double-resonant cavity configuration, and the stabilization of the cavities is required. A scheme to stabilize the cavity length at resonance with the fundamental beam is available [17].

In order to optimize the SHG enhancement, the power loss mechanism in the coupled cavities should be studied in detail. In this paper, the power loss mechanism in the macroscopic coupled cavities is studied experimentally and theoretically by the observation of the resonance curves. One of the important power loss mechanisms of the fundamental beam in the high-power range is blue-induced infrared absorption (BLIIRA) or green-induced infrared absorption [18–20]. It is suggested that the BLIIRA is an absorption process in the NLC of the infrared beam from energy states of polarons that are produced as a result of excitation of electrons in the NLC by the blue SH beam [18,21]. In the coupled-cavity configuration since the blue SH beam is enhanced substantially, the BLIIRA can be an important power loss mechanism even in the low-power range in which normally the BLIIRA is not important. In the theoretical analysis, the phase shift induced by the power loss is taken into account in addition to the BLIIRA.

## II. EXPERIMENTAL SETUP

Figure 1 is a schematic of the experimental setup. This setup is essentially the same as that of Fig. 1(b) in Ref. [16]. Two optical cavities are coupled through the NLC for the SHG (952 → 476 nm). The cavity for the fundamental beam (952 nm) consists of one input coupler (IC) and three mirrors (M1, M2, and M3), and that for the SH beam (476 nm) consists of two dichroic mirrors (DM1 and DM2) and two mirrors (M4 and M5). The dichroic mirrors are highly reflective at 476 nm and antireflective at 952 nm. For convenience, the cavities for the 952 and 476 nm are referred to as the “first cavity” and the “second cavity” hereafter, respectively. The first (second) cavity length is 34 cm (12 cm), which implies the free spectral range is 880 MHz (2.5 GHz).

The 952-nm laser beam (∼270 mW) provided by the single-mode grating-feedback external cavity laser diode followed by the tapered amplifier is coupled into the first cavity through the IC with a partial reflection coating. The reflectivity of the IC is 70%. It may seem that this condition is overcoupling, but later it turns out that the impedance-matching condition is well satisfied with this IC reflectivity. The NLC is a 10-mm-long periodically poled lithium niobate of type-0 phase matching. One of the mirrors of the first cavity (M2) is attached on a piezoelectric transducer (PZT1) for the cavity length adjustment. Similarly, M4 is attached on a piezoelectric transducer (PZT2).

*hasegawa@phys.keio.ac.jp

 

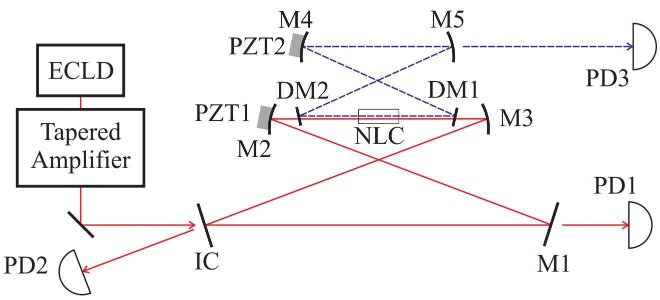


FIG. 1. (Color online) Schematic of the experimental setup.

## III. RESULTS AND DISCUSSIONS

In the experiment, the intensities of the transmitted 952-nm beam monitored with PD1, the reflected 952-nm beam monitored with PD2, and the transmitted 476-nm beam monitored with PD3 are observed as functions of the first cavity length swept by applying a triangular voltage of 10 Hz to the PZT1 (35 $\mu$m s$^{-1}$). During sweeping the first cavity length, it is close to resonance only for ~10 ms so that the power measurements at PD1, PD2, and PD3 are carried out only for 10 ms. The irrelevant change in the cavity length caused by mechanical vibrations is negligibly small during this measurement period.

During the measurement, the mechanical length of the second cavity is kept constant, and the optical cavity length can be shifted because of the optical power dependence of the refractive index of the NLC. Therefore, the optical phase shift after propagating one round of the cavity is expressed as

$$\phi_i = \delta_i + \Delta_i, \tag{1}$$

where $\delta_i$ ($i = 1$ for the first cavity and $i = 2$ for the second cavity) is the phase shift corresponding to the mechanical translation of the cavity mirror and $\Delta_i$ is the nonlinear phase shift corresponding to the change in the refractive index of the NLC. For convenience, $\delta_i$ is referred to as "mechanical phase shift," and $\Delta_i$ is referred to as "nonlinear phase shift."

In Fig. 2, the results with the conditions of the on-resonant second cavity (labeled A), off-resonant second cavity (B), and no second cavity (C) are shown. In the case of the on-resonant second cavity, the voltage applied to PZT2 is kept constant so that the highest SHG power is obtained during the sweep of the first cavity length. Therefore, the second cavity is considered to be on-resonant under the effect of the nonlinear phase shift. The case of no second cavity corresponds to the conventional cavity-enhanced SHG, and in this experiment it is accomplished by placing a beam stop between M5 and DM2 in Fig. 1. Because almost no reflection is observed in Fig. 2(b) when both cavities are on-resonant, it is expected that the impedance-matching condition is sufficiently satisfied as stated before. In order to confirm the impedance-matching condition, the reflection beam power with the use of the 80%-reflectivity IC is monitored [the inset of Fig. 2(b)] for the resonant second cavity. In this figure, a small increase (antidip) in the reflection power is observed at the resonance. This result implies that the 80% IC is for the undercoupling condition at resonance. From this result, the single round-trip loss in the first cavity can be estimated to be larger than 20% when both

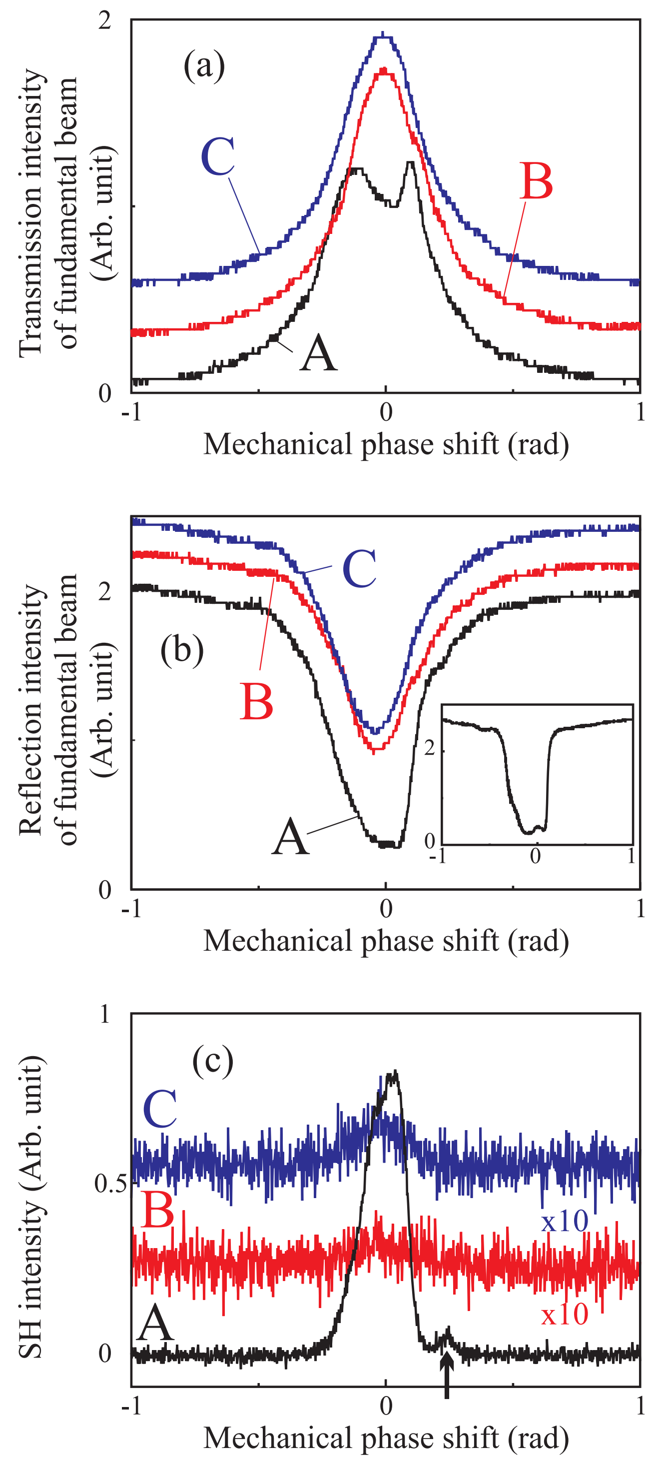


FIG. 2. (Color online) (a) Transmission intensity of the fundamental beam, (b) reflection intensity of the fundamental beam, and (c) the SH beam intensity in the coupled optical cavities when the first cavity length is swept. These values are expressed as functions of the mechanical phase shift of the first cavity. The mechanical phase shift is evaluated by the voltage applied to PZT1. The lines labeled A, B, and C represent the cases of the on-resonant second cavity, off-resonant second cavity, and no second cavity, respectively. The inset of (b) shows the reflection intensity of the fundamental beam when the 80% -reflectivity input coupler is used. For clarity, lines B and C are shifted vertically in (a)–(c) and magnified by factor of 10 in (c).

cavities are on-resonant. It should be noted that the impedance-matching condition is not satisfied (overcoupling) in the case of the off-resonant second cavity (B) or the no second cavity case (C). This result suggests that the optical power loss in the first cavity depends on the SH optical power. Discussions of this nonlinear power loss mechanism are given later.

The result in Fig. 2(c) shows that when the second cavity is on-resonant the SHG efficiency is enhanced by factor of 80 compared with the no second cavity case. The SH beam power at resonance with the no second cavity case [the peak of line C in Fig. 2(c)] is about 40 mW, and therefore the SH power in the on-resonant second cavity is expected to be $\sim$3.2 W. In addition, it is also found that the SHG is suppressed when the second cavity is off-resonant [SHG shown with line B in Fig. 2(c) is weaker than that with line C]. A small resonance identified by an arrow in Fig. 2(c) is due to the higher-order transversal Gaussian beam mode caused by the mode mismatching.

The fundamental-beam transmission line reduces at the line center (a small dip), and it is asymmetric. According to the result of the reflection power [A in Fig. 2(b)], it is shown that the impedance-matching condition for the fundamental beam is satisfied regardless of the presence of the dip. Therefore it is found that the dip is not caused by the reduction of the input coupling efficiency. We consider that the nonlinear power loss and the nonlinear phase shift stated before cause the dip and the line asymmetry in Fig. 2(a).

There can be two possibilities for the power loss. (i) At resonance, the energy in the first cavity is transferred as a SH beam power to the second cavity through the SHG, and as a result the first cavity power is depleted. (ii) At resonance, the SH beam in the second cavity is intense so that the BLIIRA is a remarkable loss mechanism. As a result, the fundamental beam is absorbed in the NLC, and the first cavity power is dissipated.

For understanding the loss mechanism in the coupled cavities in detail, a model calculation is carried out as follows. In this model, the power transfer of the fundamental beam to the SH beam by the NLC, the nonlinear power absorption by the BLIIRA process, and the nonlinear phase shift associated with the BLIIRA are considered. As stated before, the nonlinear phase shift is caused by the change in the refractive index of the NLC depending on the optical beam power. The change in the refractive index is caused by the change in the crystal temperature induced by the power loss and by the optical Kerr effect.

In the NLC, the optical field propagating along the $z$ axis from $z = 0$ to $z = L$ ($L$ is the crystal length) is expressed in the complex representation as

$$E = E_1(z)e^{i(n_1kz-\omega t)} + E_2(z)e^{2i(n_2kz-\omega t)}, \tag{2}$$

where $E_1$ and $E_2$ are the complex field amplitudes of the fundamental and the SH beams, respectively, $\omega$ is the angular frequency of the fundamental beam, $k$ is the wave number in vacuum of the fundamental beam, and $n_1$ and $n_2$ are refractive indices of the fundamental and the SH beams, respectively. Since we consider the phase-matched case only, we assume $n = n_1 = n_2$. Equation (2) is substituted into the wave equation with the nonlinear polarization term and the linear damping term [22]. With the slowly varying envelope approximation ($d^2E_{1,2}/dz^2$ is ignored), the field amplitudes satisfy

$$\frac{dE_1}{dz} + \frac{\kappa_1}{2}E_1 - \frac{i\chi^{(2)}\omega}{2nc}E_1^*E_2 = 0, \tag{3}$$

$$\frac{dE_2}{dz} + \frac{\kappa_2}{2}E_2 - \frac{i\chi^{(2)}\omega}{nc}E_1^2 = 0, \tag{4}$$

where $\kappa_1$ and $\kappa_2$ are the power damping constants of the fundamental beam and the SH beam, respectively, $\chi^{(2)}$ is the second-order susceptibility of the nonlinear crystal, and $c$ is the speed of light in vacuum. The third term of Eq. (4) corresponds to the SHG, and the third term of Eq. (3) corresponds to the power depletion of the fundamental beam by the SHG. In this analysis, we consider the power loss is due to the BLIIRA, and hence $\kappa_1$ depends on the SH power $E_2E_2^*$. Although the power saturation of the BLIIRA is observed in Ref. [20], as a first approximation, the linear dependence is assumed as $\kappa_1 = \alpha E_2(z)E_2^*(z)$ and $\kappa_2 = 0$. In addition, if $E_2(z)$ is not modified significantly in the single transmission in the NLC, it may be a good approximation to choose $\kappa_1 = \alpha E_2(0)E_2^*(0)$.

Equations (3) and (4) cannot be analytically solved. Since the purpose of this analysis is not to obtain exact numerical values, we apply another approximation to give an insight. In the present experiment, the field amplitudes of the fundamental beam and the SH beam are supposed not to change significantly in the NLC, and therefore Eqs. (3) and (4) are approximated as

$$E_1(L) = E_1(0) - \frac{\alpha E_2(0)E_2^*(0)L}{2}E_1(0) + \frac{i\chi^{(2)}\omega L}{2nc}E_1^*(0)E_2(0), \tag{5}$$

$$E_2(L) = E_2(0) + \frac{i\chi^{(2)}\omega L}{nc}E_1^2(0). \tag{6}$$

Here $dE_i(z)/dz$ is approximately replaced with $[E_i(L) - E_i(0)]/L$ ($i = 1$ or 2).

Each beam out of the crystal is fed back to the crystal around the cavity, undergoing the mechanical phase shift determined by the cavity length and the damping by the power loss at the mirrors, and so on. In addition, for the fundamental beam, the power is provided through the IC. Hence,

$$E_1(0) = r_1\gamma_1e^{i(\delta_1+\Delta_1)}E_1(L) + t_1E_0, \tag{7}$$

$$E_2(0) = \gamma_2e^{i(\delta_2+\Delta_2)}E_2(L) \tag{8}$$

should be satisfied in the stationary state, where $r_1$ and $t_1$ are the field reflectivity and the field transmittance of the IC, respectively, $\gamma_1$ and $\gamma_2$ are amplitude damping ratios of the fundamental beam and the SH beam, respectively, and $E_0$ is the input optical field. In Eqs. (7) and (8), the nonlinear phase shift at the NLC ($\Delta_i$) is also considered. The phase convention in this calculation is determined that $E_0$ is real valued. The parameters $\gamma_1$ and $\gamma_2$ represent not only the power loss at the mirrors, but also the linear damping in the NLC.

We assume that the nonlinear phase shift $\Delta_i$ is expressed as $\eta_iE_2(L)E_2^*(L)$. If the optical Kerr effect is taken into account, the nonlinear phase shift should be not only a function of $E_2$, but also a function of $E_1$. In the present analysis, however, we consider the phase shift induced by the BLIIRA only, and therefore the nonlinear phase shift is supposed to be dependent on $E_2$.

In the stationary state, Eqs. (5)–(8) are simultaneously satisfied. For the numerical calculation, the optical-field intensities are calculated as functions of the mechanical phase shift of the first cavity ($\delta_1$). In the present calculation, the parameter values are set as follows. It should be noted that the calculation is not to determine the parameter values exactly with nonlinear fitting, which is not carried out in this paper, but to confirm the effect of the BLIIRA and the nonlinear phase shift. $\chi^{(2)}$ is $1.1 \times 10^{-11}$ m V$^{-1}$, which is determined by the single-path SHG efficiency. $\alpha$ is $2 \times 10^{-11}$ m V$^{-2}$, which is estimated by the result in Ref. [18]. Because the BLIIRA coefficient strongly depends on the fabrication process of the NLCs, the value of $\alpha$ may not be exactly the same as that used in Ref. [18]. However, we expect that the value of $\alpha$ in this study is close to the estimated one. Similarly, $\eta_1 = \eta_2/2 = -2.2 \times 10^{-14}$ rad m$^2$ V$^{-2}$ is determined to agree with the result in Ref. [18]. The negative sign is chosen because in general the refractive index becomes low for higher temperatures. The mechanical phase shift of the second cavity ($\delta_2$) is kept constant during the measurement so that the highest SH power is obtained. With several trial numerical calculations, we choose $\delta_2 = 55$ mrad. $\gamma_2 = 0.985$, $\gamma_1 = 1$, $r_1 = \sqrt{0.7}$, $t_1 = \sqrt{0.3}$, and $n = 2.2$. Input field intensity $E_0$ is $\sqrt{4I_0/(\pi\varepsilon_0 c w^2)}$, supposing that $E_0$ is the center field intensity of the Gaussian beam, where $I_0$ is the input power (270 mW), $\varepsilon_0$ is the electric constant, and $w = 40$ $\mu$m is the beam radius in the NLC ($1/e^2$ in power).

Figure 3 shows the result of the numerical calculation. The fundamental beam power (a) and the SH beam power (b) are shown as functions of $\delta_1$. Solid lines represent the results with BLIIRA and the nonlinear phase shift. For comparison, the dashed lines represent the results with BLIIRA and without the nonlinear phase shift, and the dotted lines represent the results without BLIIRA and the nonlinear phase shift. In the calculations with no nonlinear phase shift (dashed lines and dotted lines), the value of $\delta_2$ is set to zero.

When the BLIIRA and the nonlinear phase shift are taken into account in the model, the calculation (solid lines) agrees well with the observation in Fig. 2. In the case of no BLIIRA and no nonlinear phase shift (dotted lines), the fundamental beam power depletion by the SHG is only considered, and in this case the dip structure cannot be reproduced. In the case of the dashed lines in Fig. 3, the dip structure of the fundamental beam transmission can be reproduced, but the asymmetric structure and the linewidth of the resonance curve do not agree with the observation. In this case, the linewidth becomes wide, and this widening is due to the increase in the power loss of the BLIIRA.

The ratio of the BLIIRA damping to the SHG conversion can be evaluated as the ratio of the second term to the third term on the right-hand side of Eq. (5), namely, $\alpha n c E_2/(\chi^{(2)}\omega)$. In the calculation, it is estimated that the SH power in the second cavity is 3.1 W at resonance, and this ratio is 0.8. From this calculation, it is found that the BLIIRA and the nonlinear phase shift associated with the BLIIRA are as significant as the SHG in the coupled-cavity configuration. Qualitatively, the

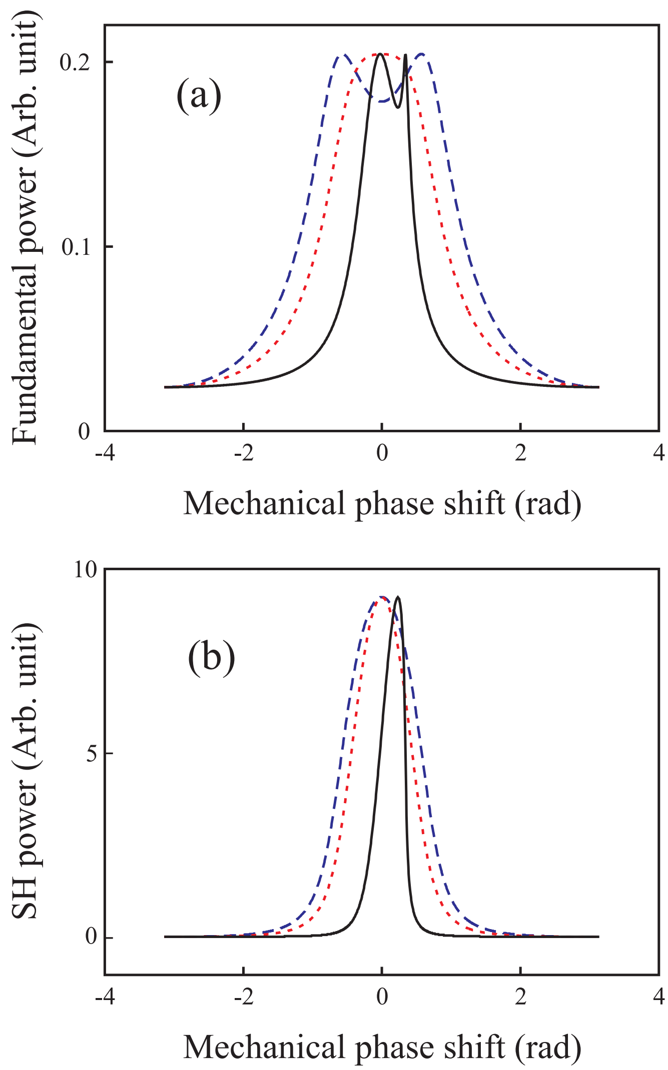


FIG. 3. (Color online) (a) Numerically calculated fundamental beam power and (b) SH beam power as functions of the mechanical phase shift of the first cavity for the case of the on-resonant second cavity. The solid lines represent the results with BLIIRA and the nonlinear phase shift, the dashed lines represent the results with BLIIRA and without the nonlinear phase shift, and the dotted lines represent the results without BLIIRA and the nonlinear phase shift. The plots are normalized to the peak power.

BLIIRA causes the dip structure, and the asymmetric distortion of the line shape is caused by the nonlinear phase shift for the fundamental beam.

The line narrowing of the solid line in Fig. 3(a) is qualitatively understood as follows. The value of $\delta_2$ is chosen to compensate the nonlinear phase shift. Only when the compensation works well, the second cavity is on-resonant, and the SH beam power is intense. Therefore, the resonance of the second cavity occurs within the narrow range of the mechanical phase shift of the first cavity (the range is determined by the values of $\delta_2$ and $\eta_2$). If $\delta_1$ is out of this range, the SH power is not intense because the second cavity is off-resonant, and therefore the BLIIRA is not significant. As a result, the power loss in the first cavity is small, and the linewidth becomes narrow.

The thermal effect by the BLIIRA causes not only the nonlinear phase shift, but also phase mismatching of the SHG in the NLC and a thermal lens effect (photorefractive effect). Further discussions for these effects are for future papers. In addition, the saturation effect of the BLIIRA [20] should be taken into account for further discussions.

## IV. CONCLUSIONS

In conclusion, the optical powers of the fundamental beam and the SH beam in the coupled cavities are observed in detail to study the power loss mechanism and the nonlinear phase shift. In the experiment, the SH beam intensity is enhanced by a factor of 80 by the second cavity. By theoretical analysis, it is found that there are two power loss mechanisms of the fundamental beam, namely, power transfer to the SH beam and the BLIIRA. The single round-trip power loss ratio of the fundamental beam is estimated as over 20% from the impedance-matching condition. In the coupled-cavity configuration, the BLIIRA and the associated nonlinear phase shift are important since the SH beam is significantly enhanced in the second cavity. In order to reduce the power loss by the BLIIRA in the coupled-cavity configuration, NLCs with less BLIIRA, such as lithium triborate and periodically poled $KTiOPO_4$ should be used so that efficient fourth-harmonic generation is expected.


[1] C. Zimmermann, R. Kallenbach, T. W. Hänsch, and J. Sandberg, Opt. Commun. **71**, 229 (1989).

[2] V. Berger, J. Opt. Soc. B **14**, 1351 (1997).

[3] K. Fiedler, S. Schiller, R. Paschotta, P. Kürz, and J. Mlynek, Opt. Lett. **18**, 1786 (1993).

[4] P. S. Kuo, J. Bravo-Abad, and G. S. Solomon, Nat. Commun. **5**, 3109 (2014).

[5] K. Rivoire, Z. Lin, F. Hatami, W. T. Masselink, and J. Vuckovic, Opt. Express **17**, 22609 (2009).

[6] T. Dolgova, A. Maidykovski, M. Martemyanov, A. Fedyanin, O. Aktsipetrov, G. Marowsky, V. Yakovlev, and G. Mattei, Appl. Phys. Lett. **81**, 2725 (2002).

[7] V. Berger, X. Marcadet, and J. Nagle, Pure Appl. Opt. **7**, 319 (1998).

[8] C. Simonneau, J. Debray, J. Harmand, P. Vidakovic, D. Lovering, and J. Levenson, Opt. Lett. **22**, 1775 (1997).

[9] Z.-F. Bi, A. Rodriguez, H. Hashemi, D. Duchesne, M. Loncar, K.-M. Wang, and S. G. Johnson, Opt. Express **20**, 7526 (2012).

[10] M. Liscidini and L. C. Andreani, Phys. Rev. E **73**, 016613 (2006).

[11] Y. Dumeige and P. Féron, Phys. Rev. A **74**, 063804 (2006).

[12] M. Liscidini and L. C. Andreani, Appl. Phys. Lett. **85**, 1883 (2004).

[13] A. Rodriguez, M. Soljacic, J. D. Joannopoulos, and S. G. Johnson, Opt. Express **15**, 7303 (2007).

[14] Z. Y. Ou and H. J. Kimble, Opt. Lett. **18**, 1053 (1993).

[15] K. Stoll, J. J. Zondy, and O. Acef, Opt. Lett. **22**, 1302 (1997).

[16] T. Hasegawa, Opt. Commun. **285**, 5368 (2012).

[17] T. Hasegawa, Opt. Commun. **308**, 270 (2013).

[18] Y. Furukawa, K. Kitamura, A. Alexandrovski, R. K. Route, M. M. Fejer, and G. Foulon, Appl. Phys. Lett. **78**, 1970 (2001).

[19] H. Mabuchi, E. S. Poizik, and H. J. Kimble, J. Opt. Soc. Am. B **11**, 2023 (1994).

[20] N. Waasem, A. Markosyan, M. M. Fejer, and K. Buse, Opt. Lett. **38**, 2953 (2013).

[21] S. Enomoto and S. Ashihara, J. Appl. Phys. **110**, 063111 (2011).

[22] A. Yariv and P. Yeh, *Photonics: Optical Electronics in Modern Communications* (Oxford University Press, Oxford, 2006).